Finite Nanostructures

DOI: 10.1002/ange.201303135

Templated Hierarchical Self-Assembly of Poly(*p*-aryltriazole) Foldamers**

Rueben Pfukwa, Paul H. J. Kouwer, Alan E. Rowan, and Bert Klumperman**

Dynamic equilibrium conditions in biological self-assembly lead to efficient information transfer and self-regulation.[1] To implement equilibrium self-assembly, and create large finite nanostructures, there is a need to utilize building blocks with well-characterized and predictable conformational behavior. Foldamers are ideal models for understanding the folding and hierarchical self-assembly of biopolymers, owing to the predictability of their folding behavior and the relative ease of their synthesis.[2] A popular design of synthetic foldamers is based on aromatic rings, joined by rigid linking groups such as acetylenes,[3] amides,[2d,4] ureas,[5] and triazoles.[6] More recent research on these "aryl-rigid linker" foldamer systems is directed at forming more advanced architectures than mere helices and at the introduction of functionality.[7] For these systems, however, a full description of the conformational intermediates between the unfolded and fully folded conformations is often still lacking. The characterization of the intermediates involved in the folding process allows for increased understanding and, more importantly, gives the opportunity to control and manipulate the self-assembly process more precisely. Herein, we describe a new helicity codon based on a *para*-linked aryltriazole system, where we are able to fully characterize the conformational transition processes. We show that the intermediate conformations are the ideal starting point for controlled hierarchical assembly and we demonstrate this concept by using macromolecular templating in the construction of well-defined assemblies of finite dimensions and helicity,[8] much like the controlled assembly of tobacco mosaic virus (TMV).[9]

In our poly(*para*-aryltriazole) [P(*p*-AT)] system, a crescent shape is induced by adopting a 1,4-disubstitution pattern of the triazole ring. In combination with an extended *cisoid* conformation (Scheme 1a) the crescent shape enforces helical folding in P(*p*-AT)s with a sufficiently large degree of polymerization. Molecular modeling predicted a helical conformation with 14.5 repeat units per turn, and a large internal diameter of approximately 30.6 Å (Scheme 1b). In the helically folded conformation, each aryl ring has a triazole ring stacked above and below it. The distance between turns is approximately 3.8 Å, which is consistent with the turns of the helix being near van der Waals contact.[10] The large cavity of the helix is a direct consequence of linking the aryltriazole units, exclusively, in a *para* geometry on the benzene ring. This reduces the curvature of the backbone and many repeat units are required to complete one turn. The aryltriazole linkage has been shown to adopt a flat conformation,[2c,11] and thus when it folds, the torsion is spread over many aryltriazole links as illustrated by the extensive inter-ring co-planarity (Scheme 1b).

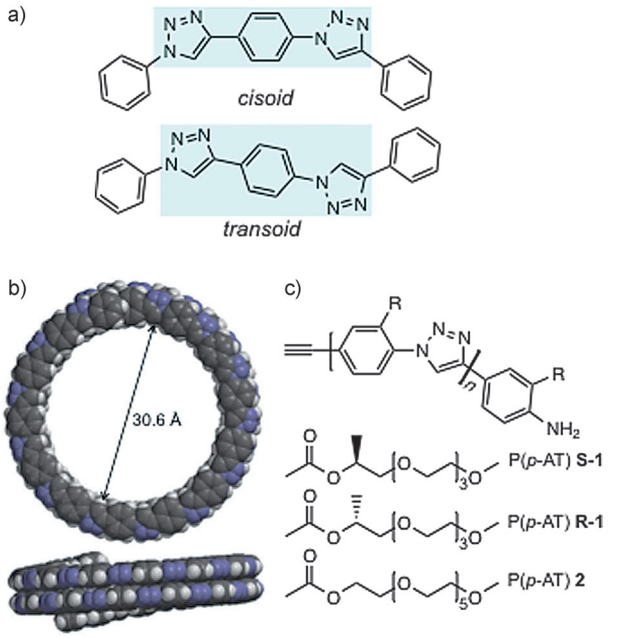

Scheme 1. a) Helicity codon, b) calculated helix, and c) P(*p*-AT) general structure.

P(*p*-AT)s ***S*-1**, ***R*-1**, and **2** (Scheme 1c) with oligo(ethylene glycol) substituents were designed to switch conformations in different solvent environments (for the synthesis, see the

[*] Dr. R. Pfukwa, Prof. B. Klumperman
Stellenbosch University
Department of Chemistry and Polymer Science
Private Bag X1, Matieland 7602 (South Africa)
E-mail: bklump@sun.ac.za
Homepage: http://www.klumperman-group.net/
Dr. P. H. J. Kouwer, Prof. A. E. Rowan
Institute of Molecular Materials, Radboud University Nijmegen
Heyendaalseweg135, 6525 AJ, Nijmegen (The Netherlands)
E-mail: a.rowan@science.ru.nl

[**] This work was supported by the South African Research Chairs Initiative (SARChI) from the Department of Science and Technology (DST), the National Research Foundation (NRF), the Council for the Chemical Sciences of the Netherlands Organisation for Scientific Research, and the EU (ITN Hierarchy, contract PITN-2007-215851). R.P. thanks the Marie Curie Fellowship for financial support. We thank Rinske Knoop for the TEM and cryoTEM images, and Franscious Cummings for the TEM images.

Supporting information for this article is available on the WWW under http://dx.doi.org/10.1002/anie.201303135.

Supporting Information, Scheme S1).[6a,12] Enantiopure chiral side chains were installed on P(*p*-AT)s ***S*-1** and ***R*-1** to direct the screw-sense of the helical assemblies.[13] Of the many available techniques to study folding behavior,[13a,14] we used UV/Vis and CD spectroscopy to track solvent dependent conformational changes and to identify intermediate structures of the folding process.

Spectroscopic signatures of folding were determined from solutions of P(*p*-AT) ***S*-1** in DMF/water (non-selective/selective solvent, respectively). The random coil, which prevails in DMF, is characterized by a UV peak at 284 nm and a shoulder at 310 nm, and is CD silent (red spectra, Figure 1 a). From 10 % v/v water in DMF (10 % H_2O), the

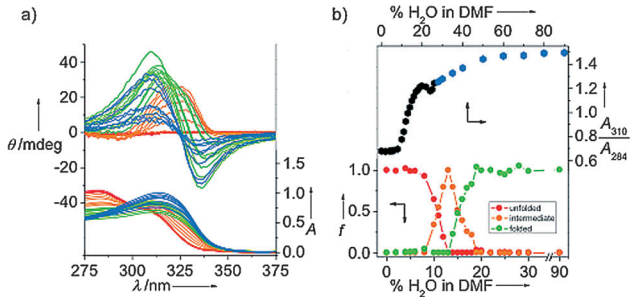

Figure 1. a) UV (bottom) and CD spectra (top) of the solvent titrations of P(*p*-AT)-***S*-1**; b) plots of the UV absorbance ratio (A_{310}/A_{284}) (top) and equilibrium populations of various conformational species (bottom) as a function of solvent composition.

shoulder peak at about 310 nm increases in intensity whilst the peak at 284 nm decreases (orange UV spectra, Figure 1 a), and at 13 % H_2O, the peaks at 284 and 310 nm have equal intensities. With further increments of water the peak at 310 nm increases and red shifts, whilst the peak at 284 nm attenuates. The plot of the ratio of the UV bands at 310 nm and 284 nm (A_{310}/A_{284}), as a function of solvent composition[3a] reveals two distinct regimes (Figure 1 b). From 0 % to about 25 % H_2O (black dots), the plot is sigmoidal, a characteristic of cooperative conformational transitions.[14d,15] After the plateau from about 28 % H_2O onwards, the ratio steadily increases again, leveling off at high water fractions.

In the CD spectra, a single positive Cotton effect appears at 10 % H_2O (orange spectra), growing in intensity with increasing water content. At about 20 % H_2O, the Cotton effect, however, evolved into a bisignate signal exhibiting negative exciton chirality, with an isodichroic point at 330 nm suggesting the formation of a helical conformation with preferred handedness owing to chirality transfer from the side chain to the backbone (green spectra).[13] From 20 % H_2O, the amplitude of the Cotton effect further increases with increasing H_2O content, peaking at 28 % H_2O. The isodichroic point shifts to 325 nm. Upon further increase of the water fraction beyond 28 % H_2O the amplitude of the Cotton effect decreases,[16] but the isodichroic point does not change (blue spectra).

The formation of a single clear bisignate Cotton effect at 20 % H_2O indicates that the coil-to-helix transition is completed and the polymer is in a well-defined helical conformation. In the transition regime, however, the polymer, which shows the positive Cotton effect, is not as well defined and we describe its conformation as a "loose spring" (Scheme 2). As the two conformations are spectroscopically

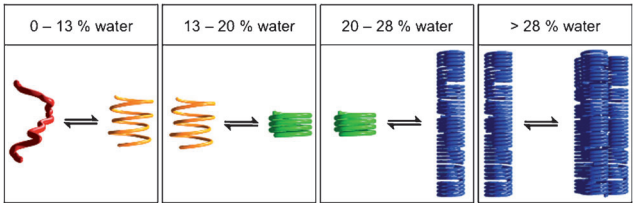

Scheme 2. Solvent-dependent hierarchical self-assembly pathway of P(*p*-AT)s, illustrating the key conformational structures. The color code is linked to the colors in Figure 1.

clearly resolved, we deconvoluted the UV spectra and obtained a profile of the equilibrium conformational populations as a function of solvent composition (Figure 1 b). The analysis shows that at low water content, random coil and "loose spring" conformations are in equilibrium; at intermediate water content, "loose springs" and stable helices are in equilibrium. In fact, we do not observe a region where random coils and stable helices coexist. The inflection point, at 13 % water, marks the coil-to-helix transition midpoint with the loose spring as the dominant conformation. Spectroscopic resolution of intermediate conformers is unprecedented for amphiphilic "aryl-rigid linker" foldamers. We expect this conformation to be very dynamic and also sensitive towards changes in its environment, which makes it the ideal starting point for further hierarchical assembly processes. The increase in amplitude of the CD couplet and the red-shifts of the isodichroic point and the UV band at 310 nm between 20–28 % water is explained as a further tightening of the stable helical conformation.

Beyond 28 % H_2O, the UV analysis shows an upswing in the A_{310}/A_{284} plot whereas the CD signal decreases, owing to kinetic trapping[16] (Figure 1 a,b, top, respectively). This suggests that at high water content, the intramolecular structure of the helices stays intact, but that the molecules now start assembling into a tertiary structure, that is, nanotubes.[17] TEM and cryoTEM analyses of P(*p*-AT) ***S*-1** show convincing evidence for the formation of helical columns, formed by stacked helices, which further aggregate into bundles and coils (Figure 2 a,b).

The UV and CD spectra of P(*p*-AT)s ***R*-1** and **2** as a function of solvent composition evolve analogously to P(*p*-AT) ***S*-1** (Supporting Information, Figures S8 and S9), indicating that they follow the same hierarchical pathway. As expected, the Cotton effects of P(*p*-AT)s ***S*-1** and ***R*-1** are exact mirror images (Supporting Information, Figure S8E), which demonstrates that these helical foldamers have preferred, and opposite, twist sense biases imparted by their chiral side chains.[13] The longer oEG side chain in P(*p*-AT) **2** gives rise to an increased solubility in water and thus slightly weaker solvophobic interactions. This shifts the coil-to-helix transition midpoint to 19 % H_2O and the formation of higher-order structures starts at about 40 % H_2O (Supporting

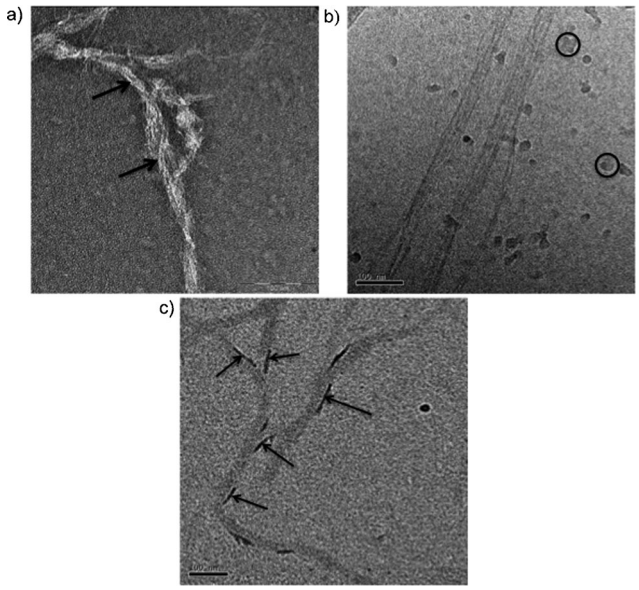

Figure 2. a) TEM image of P(*p*-AT) ***S*-1** [1.11 μM], prepared from 80% H_2O; b) CryoTEM image of P(*p*-AT) **2** [29.8 μM] prepared from 100% H_2O. The irregular shaped blots (some are circled) are ice crystals contaminating the surface of the sample; c) the self-assembled complex of P(*p*-AT) **2** with PBLG **B**, which shows nanostructures with lengths of 62.8 ± 9.1 nm.

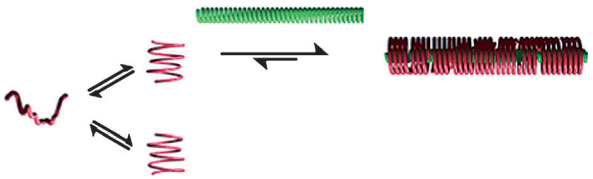

Scheme 3. Proposed diastereoselective templated self-assembly of P(*p*-AT) **2**.

Information, Figure S9). Cryo-TEM experiments using the achiral P(*p*-AT) **2** at high water content confirm the formation of solution stable tertiary structures (Figure 2b; Supporting Information, Figure S12). The helices stack into long columns of varying lengths.

The assembly process thus far follows classical hierarchical foldamer organization where stack formation and length are thermodynamically controlled.[6d,17] To direct this assembly process to yield well-defined structures, we used a polymer template. This approach is inspired by nature, which applies it in the self-assembly of, for instance, the tobacco mosaic virus (TMV). TMV is an asymmetric rod-shaped virus comprised of protein capsids encasing a single RNA strand that regulates the length and chirality of the virus complex.[9b] We chose the rigid and hydrophobic poly(γ-benzyl-L-glutamate) (PBLG) α-helix as our RNA mimic. The stiff polymer has a diameter of about 1.6 nm,[18] which matches well with the calculated helical cavity,[19] and its hydrophobic nature is expected to drive the assembly. As the starting point we investigated the influence of the template at the coil-to-helix transition midpoint, which for P(*p*-AT) **2** is 18% H_2O (Scheme 3).

Evidence for chiral information transfer between the achiral P(*p*-AT) **2** and the chiral PBLG was obtained by CD spectroscopy (Figure 3a). A negative bisignate Cotton effect is observed in the wavelength region where only the P(*p*-AT) **2** absorbs, which points to an enantiomeric excess of one of both helices as a result of macromolecular templating. Two control experiments, either with P(*p*-AT) **2** in the random-coil conformation (0% H_2O) or without the template present, showed no chiral expression of the foldamer (Figure 3a).

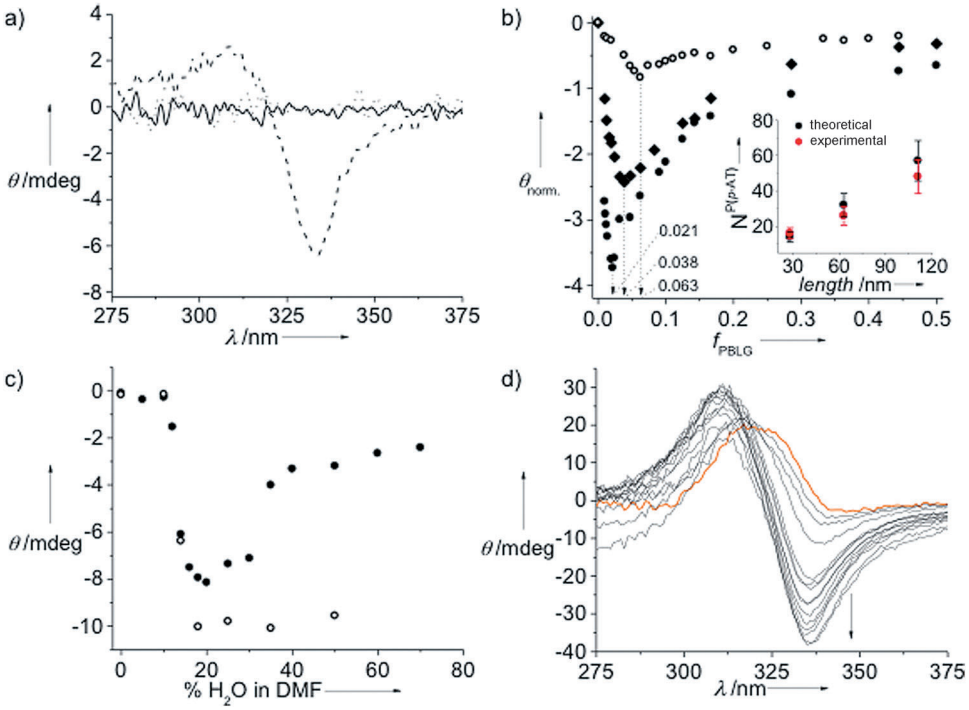

Figure 3. a) CD spectra of P(*p*-AT) **2** and PBLG **B** in 100% DMF (——) and in 18% H_2O (-----), and P(*p*-AT) **2** alone in 18% H_2O (••••); B) Job plot of P(*p*-AT) **2** and PBLG **A**-**C** (● **A**, ◆ **B**, ○ **C**) to determine the stoichiometry of the inclusion complex (inset: plot of stoichiometric ratio versus template length: black = theoretical, red = experimental); c) plot of CD activity at 333 nm versus solvent composition for the stoichiometric complex of P(*p*-AT) **2** and PBLG **B** (● "quick", ○ "slow" water addition); d) evolution of CD spectra with increasing template concentration for inclusion complex P(*p*-AT) ***S*-1** and PBLG **B** (orange curve = P(*p*-AT) ***S*-1** without PBLG template).

Length information transfer is demonstrated via a length dependent templating effect. CD titrations of three PBLG templates of differing length (PBLG **A**, **B**, and **C**) were carried out. A subsequent Job plot analysis (Figure 3b) showed that the stoichiometry of the complexes closely correspond to what can be expected considering the molecular weights (that is, lengths) of the templates (Supporting Information, Table S5) and the (modeled) packing distance of the stable helix. Indeed, the linear increase of the average number of foldamers $N^{P(p\text{-AT})2}$ with the length of the template shows a direct analogy to the length-dependent templating effect of TMV.

The hypothesis that templating is most effective from the coil-to-helix transition midpoint of the foldamers was tested by measuring the CD signals of stoichiometric complexes prepared at various volume fractions of water (Figure 3c). Below 10% water, no CD signal is observed as the foldamer is unfolded. The highest CD signals are observed from 18-20% water in DMF, around the coil-to-helix transition midpoint of the foldamer, where P(*p*-AT) **2** forms a racemic mixture of left and right handed "loose springs". The template then interacts more favorably with the foldamer helix with a matching screw sense, which biases the system towards the chiral complex (Scheme 3). Above 25% water, however, depending on the rate of addition of the selective solvent (water), the intensity of the CD effect either remains constant (slow water addition) or reduces. At higher water compositions (>18%), rapid water addition results in the kinetic trapping of the racemate of left and right-handed helices, causing the CD effect of the uncomplexed non-matching helices to gradually increase, leading to a reduction of the overall CD intensity. Under these conditions, however, we also cannot exclude that a significant fraction of the non-matching foldamer helices will be threaded on the template, albeit with lower energy benefits than the matching counterparts.

It is clear that the template modifies the hierarchical self-assembly pathway. Non-templated self-assembly follows a step-wise process, characterized by different regimes in the A_{310}/A_{284} plot (Figure 1b). With a template present, however, foldamer assembly begins as soon as the "loose springs" are formed. Additional interactions between the template and the foldamer stabilize the stable helix along with the intermolecular interactions. As a result, the corresponding A_{310}/A_{284} plot shows that the plateau and second rise is smoothed out in the presence of the template (Supporting Information, Figure S16).

CD titrations of PBLG to the chiral P(*p*-AT) ***S*-1** give the same picture.[20] At its coil-to-helix transition midpoint, the CD spectrum shows a single positive Cotton effect (Figure 3d). As more template **B** is introduced, the positive Cotton signal evolves to a full bisignate negative couplet, corresponding to the transition of the loose springs to stable helices.

Further evidence of this template-induced stabilization is provided by TEM experiments. Whilst the non-templated pathway yielded long stacks and bundles of helices on the grids (Figure 2a,b), the samples with template B (length ca. 60 nm) present showed well-defined nanostructures of matching length, 62.8 ± 9.1 nm (Figure 2c).

In conclusion, we presented a new TMV mimic composed of 1,4-aryl-disubstituted-1,2,3-triazoles foldamers and α-helical PBLG templates. Assembly studies in the absence of the template revealed the intermediate conformations between a random coil and hierarchically built-up (helical) bundles. In fact, full spectroscopic resolution allowed us to profile the populations of the intermediates. The template then transfers both chiral and dimensional information onto the foldamer, in the process changing the thermodynamics of the foldamer assembly process. Our studies clearly show that the information transfer is most effective right at the coil-to-helix transition midpoint. Current on-going studies are focused on understanding the kinetics of the templated self-assembly.

Received: April 15, 2013
Revised: July 23, 2013
Published online: September 3, 2013

Keywords: biomimetic synthesis · foldamers · information transfer · self-assembly · template

[1] a) G. M. Whitesides, J. P. Mathias, C. T. Seto, *Science* **1991**, *254*, 1312–1319; b) J. S. Lindsey, *New J. Chem.* **1991**, *15*, 153–180.
[2] a) I. Huc, S. Hecht, *Foldamers: Functions, Structure, Properties, and Applications*, Wiley-VCH, Weinheim, **2007**; b) D. J. Hill, M. J. Mio, R. B. Prince, T. S. Hughes, J. S. Moore, *Chem. Rev.* **2001**, *101*, 3893–4012; c) D. Zornik, R. M. Meudtner, T. El Malah, C. M. Thiele, S. Hecht, *Chem. Eur. J.* **2011**, *17*, 1473–1484; d) D.-W. Zhang, X. Zhao, J.-L. Hou, Z.-T. Li, *Chem. Rev.* **2012**, *112*, 5271–5316.
[3] a) J. C. Nelson, J. G. Saven, J. S. Moore, P. G. Wolynes, *Science* **1997**, *277*, 1793–1796; b) M. T. Stone, J. M. Heemstra, J. S. Moore, *Acc. Chem. Res.* **2005**, *38*, 11–20.
[4] B. Gong, *Acc. Chem. Res.* **2008**, *41*, 1376–1386.
[5] J. J. van Gorp, J. A. J. M. Vekemans, E. W. Meijer, *Chem. Commun.* **2004**, 60–61.
[6] a) R. M. Meudtner, S. Hecht, *Angew. Chem.* **2008**, *120*, 5004–5008; *Angew. Chem. Int. Ed.* **2008**, *47*, 4926–4930; b) H. Juwarker, J. M. Lenhardt, D. M. Pham, S. L. Craig, *Angew. Chem.* **2008**, *120*, 3800–3803; *Angew. Chem. Int. Ed.* **2008**, *47*, 3740–3743; c) Y. Li, A. H. Flood, *J. Am. Chem. Soc.* **2008**, *130*, 12111–12122; d) Y. Wang, F. Li, Y. Han, F. Wang, H. Jiang, *Chem. Eur. J.* **2009**, *15*, 9424–9433.
[7] a) N. Delsuc, S. Massip, J. M. Léger, B. Kauffmann, I. Huc, *J. Am. Chem. Soc.* **2011**, *133*, 3165–3172; b) Y. Hua, A. H. Flood, *J. Am. Chem. Soc.* **2010**, *132*, 12838–12840; c) W. Minoru, A. Hajime, I. Masahiko, *Chem. Eur. J.* **2006**, *12*, 7839–7847; d) H. Juwarker, J. Suk, K. Jeong, *Chem. Soc. Rev.* **2009**, *38*, 3316–3325; e) C. M. Goodman, S. Choi, S. Shandler, W. F. DeGrado, *Nat. Chem. Biol.* **2007**, *3*, 252–262; f) G. Guichard, I. Huc, *Chem. Commun.* **2011**, *47*, 5933–5941; g) Y. Ferrand, A. M. Kendhale, B. Kauffmann, A. Grelard, C. Marie, V. Blot, M. Pipelier, D. Dubreuil, I. Huc, *J. Am. Chem. Soc.* **2010**, *132*, 7858–7859; h) R. A. Smaldone, J. S. Moore, *Chem. Eur. J.* **2008**, *14*, 2650–2657.
[8] a) A. Petitjean, L. A. Cuccia, M. Schmutz, J.-M. Lehn, *J. Org. Chem.* **2008**, *73*, 2481–2495; b) V. Berl, M. J. Krische, I. Huc, J.-M. Lehn, M. Schmutz, *Chem. Eur. J.* **2000**, *6*, 1938–1946; c) Q. Gan, Y. Ferrand, C. Bao, B. Kauffmann, A. Grelard, H. Jiang, I. Huc, *Science* **2011**, *331*, 1172–1175; d) Y. Ferrand, Q. Gan, B. Kauffmann, H. Jiang, I. Huc, *Angew. Chem.* **2011**, *123*, 7714–

7717; *Angew. Chem. Int. Ed.* **2011**, *50*, 7572 – 7575; e) Q. Gan, Y. Ferrand, N. Chandramouli, B. Kauffmann, C. Aube, D. Dubreuil, I. Huc, *J. Am. Chem. Soc.* **2012**, *134*, 15656 – 15659; A. Tanatani, T. S. Hughes, J. S. Moore, *Angew. Chem.* **2002**, *114*, 335 – 338; *Angew. Chem. Int. Ed.* **2002**, *41*, 325 – 328.

[9] a) A. Klug, *Angew. Chem.* **1983**, *95*, 579 – 596; *Angew. Chem. Int. Ed. Engl.* **1983**, *22*, 565 – 582; b) A. Klug, *Philos. Trans. R. Soc. London Ser. B* **1999**, *354*, 531 – 535.

[10] a) O.-S. Lee, J. G. Saven, *J. Phys. Chem. B* **2004**, *108*, 11988 – 11994; b) R. F. Kelley, B. Rybtchinski, M. T. Stone, J. S. Moore, M. R. Wasielewski, *J. Am. Chem. Soc.* **2007**, *129*, 4114 – 4115.

[11] a) B. M. J. M. Suijkerbuijk, B. N. H. Aerts, H. P. Dijkstra, M. Lutz, A. L. Spek, G. v. Koten, R. J. M. K. Gebbink, *Dalton Trans.* **2007**, 1273 – 1276; b) Y. Li, A. H. Flood, *Angew. Chem.* **2008**, *120*, 2689 – 2692; *Angew. Chem. Int. Ed.* **2008**, *47*, 2649 – 2652; c) Y.-Y. Zhu, G.-T. Wang, R.-X. Wang, Z.-T. Li, *Cryst. Growth Des.* **2009**, *9*, 4778 – 4783.

[12] D. J. Hill, J. S. Moore, *Proc. Natl. Acad. Sci. USA* **2002**, *99*, 5053 – 5057.

[13] a) R. B. Prince, L. Brunsveld, E. W. Meijer, J. S. Moore, *Angew. Chem.* **2000**, *112*, 234 – 236; *Angew. Chem. Int. Ed.* **2000**, *39*, 228 – 230; b) R. B. Prince, J. S. Moore, L. Brunsveld, E. W. Meijer, *Chem. Eur. J.* **2001**, *7*, 4150 – 4154; c) M. Banno, T. Yamaguchi, K. Nagai, C. Kaiser, S. Hecht, E. Yashima, *J. Am. Chem. Soc.* **2012**, *134*, 8718 – 8728.

[14] For representative examples of techniques used to characterize foldamers in the solution state (NMR spectroscopy, SAXS, spin labeling, single-molecule spectroscopy; fluorescence spectroscopy, UV/Vis spectroscopy, and CD spectroscopy), see Ref. [10b] and: a) C. Dolain, A. Grélard, M. Laguerre, H. Jiang, V. Maurizot, I. Huc, *Chem. Eur. J.* **2005**, *11*, 6135 – 6144; b) K. Matsuda, M. T. Stone, J. S. Moore, *J. Am. Chem. Soc.* **2002**, *124*, 11836 – 11837; c) J. J. Han, W. Wang, A. D. Q. Li, *J. Am. Chem. Soc.* **2005**, *127*, 672 – 673; d) R. B. Prince, J. G. Saven, P. G. Wolynes, J. S. Moore, *J. Am. Chem. Soc.* **1999**, *121*, 3114 – 3121.

[15] a) C. R. Ray, J. S. Moore, *Adv. Polym. Sci.* **2005**, *177*, 91 – 149; b) Y. Zhao, J. S. Moore in *Foldamers: Structure, Properties, and Applications* (Eds.: S. Hecht, I. Huc), Wiley-VCH, Weinheim, **2007**, pp. 75 – 108.

[16] The decrease in the CD intensity at high water percentages (> 28 %) results from the trapping of the foldamer in helices of opposite handedness that cannot revert. This kinetic trapping is a manifestation of the sample preparation, which entails a rapid pipetting of water (selective solvent) into the DMF solution of the P(*p*-AT), and it can be overcome by slowly adding water (see the Supporting Information).

[17] a) L. Brunsveld, E. W. Meijer, R. B. Prince, J. S. Moore, *J. Am. Chem. Soc.* **2001**, *123*, 7978 – 7984; b) L. A. Cuccia, J.-M. Lehn, J.-C. Homo, M. Schmutz, *Angew. Chem.* **2000**, *112*, 239 – 243; *Angew. Chem. Int. Ed.* **2000**, *39*, 233 – 237.

[18] S. Lecommandoux, M.-F. Achard, J. F. Langenwalter, H.-A. Klok, *Macromolecules* **2001**, *34*, 9100 – 9111.

[19] A favourable recognition event is expected when the guest occupies about 55 % of the host cavity; see: S. Mecozzi, J. Rebek, *Chem. Eur. J.* **1998**, *4*, 1016 – 1022.

[20] Enantioselectivity tests showed that PBLG selectively complexes with P(*p*-AT)-**8a** (which displays M helicity) foldamer and not the P-P(*p*-AT)-**8b** (which displays P helicity); see the Supporting Information.

